



Net optical parametric gain in a submicron silicon core fiber pumped in the telecom band

Cite as: APL Photonics 4, 086102 (2019); <https://doi.org/10.1063/1.5103272>

Submitted: 25 April 2019 . Accepted: 12 August 2019 . Published Online: 26 August 2019

Dong Wu, Li Shen, Haonan Ren, Joseph Campling, Thomas W. Hawkins, John Ballato , Ursula J. Gibson , and Anna C. Peacock



View Online



Export Citation



CrossMark

ARTICLES YOU MAY BE INTERESTED IN

Nonlinear elasticity of silica nanofiber


APL Photonics 4, 080804 (2019); <https://doi.org/10.1063/1.5103239>

Hybrid plasmonic waveguide coupling of photons from a single molecule

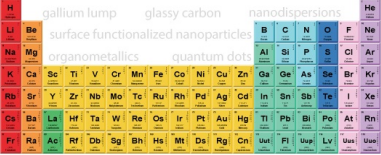
APL Photonics 4, 086101 (2019); <https://doi.org/10.1063/1.5110275>

Electromechanical Brillouin scattering in integrated planar photonics

APL Photonics 4, 080802 (2019); <https://doi.org/10.1063/1.5108672>



THE ADVANCED MATERIALS MANUFACTURER®



additive manufacturing epitaxial crystal growth cerium oxide polishing powder silver nanoparticles sputtering targets III-IV semiconductors CVD precursors europium phosphors

deposition slugs OLED Lighting spintronics solar energy osmium nanoribbons thin films chalcogenides AuNPs GDC Li-ion battery electrolytes 99.999% ruthenium spheres

endohedral fullerenes copper nanoparticles diamond micropowder CIGS MBE grade materials palladium catalysts flexible electronics YBCO

pyrolytic graphite 3d graphene foam indium tin oxide mesoporous silica raman substrates sapphire windows tungsten carbide InGaAs barium fluoride carbon nanotubes lithium niobate scandium powder

gallium lump glassy carbon nanodispersions InAs wafers laser crystals ultra high purity materials MOFs surface functionalized nanoparticles organometallics quantum dot Al Si P S Cl Ar rare earth metals photovoltaics refractory metals MOCVD superconductors transparent ceramics ultra high purity silicon

American Elements opens up a world of possibilities so you can **Now Invent!**

Over 15,000 certified high purity laboratory chemicals, metals, & advanced materials and a state-of-the-art Research Center. Printable GHS-compliant Safety Data Sheets. Thousands of new products. And much more. All on a secure multi-language "Mobile Responsive" platform.

perovskite crystals yttrium iron garnet alternative energy h-BN gold nanocubes graphene oxide macromolecules photonics rhodium sponge fiber optics beamsplitters infrared dyes zeolites fused quartz metallocenes platinum ink buckyballs Ti-6Al-4V

Now Invent.™
The Next Generation of Material Science Catalogs

www.americanelements.com

Net optical parametric gain in a submicron silicon core fiber pumped in the telecom band

Cite as: APL Photon. 4, 086102 (2019); doi: 10.1063/1.5103272

Submitted: 25 April 2019 • Accepted: 12 August 2019 •

Published Online: 26 August 2019



Dong Wu,¹ Li Shen,^{1,a)} Haonan Ren,¹ Joseph Campling,¹ Thomas W. Hawkins,² John Ballato,²  Ursula J. Gibson,^{3,b)}  and Anna C. Peacock¹

AFFILIATIONS

¹Optoelectronics Research Centre, University of Southampton, Southampton SO17 1BJ, United Kingdom

²Center for Optical Materials Science and Engineering Technologies and Department of Materials Science and Engineering, Clemson University, Clemson, South Carolina 29634, USA

³Department of Physics and Porelabs, Norwegian University of Science and Technology, N-7491 Trondheim, Norway

^{a)}Also at: Wuhan National Laboratory for Optoelectronics, Huazhong University of Science and Technology, Wuhan 430074, China. **Electronic mail:** L.Shen@soton.ac.uk.

^{b)}Also at: Department of Applied Physics, KTH Royal Institute of Technology, Stockholm 10044, Sweden.

ABSTRACT

A silicon core fiber (SCF) has been designed and fabricated with a dispersion engineered profile to support broadband optical parametric amplification across the telecom window. The combination of low optical transmission losses and high coupling efficiency of the SCF platform has allowed for an on-off optical parametric gain up to 9 dB, without experiencing gain saturation due to nonlinear absorption, resulting in a net off-waveguide gain of ~2 dB. The ability to splice the SCFs with conventional silica fiber systems opens a route to compact and robust all-fiber integrated optical parametric amplifiers and oscillators that could find use in telecoms systems.

© 2019 Author(s). All article content, except where otherwise noted, is licensed under a Creative Commons Attribution (CC BY) license (<http://creativecommons.org/licenses/by/4.0/>). <https://doi.org/10.1063/1.5103272>

I. INTRODUCTION

Over the past two decades, optical parametric amplification (OPA) based on four-wave mixing (FWM) has been studied extensively as a means to generate and amplify information signals over a broad wavelength range for communications networks.¹ Although many of the initial investigations employed high-nonlinearity silica-based fibers owing to their immediate compatibility with existing fiber infrastructures,² over the past decade silicon nanophotonic waveguides produced from the silicon-on-insulator (SOI) platform have emerged as an interesting alternative.³ Compared to the fibers, these on-chip waveguides offer useful advantages in that, owing to their significantly larger nonlinear coefficients, they are extremely compact and offer much lower power thresholds. As a result, various FWM-based demonstrations have been reported in silicon waveguides ranging from the transfer,^{4–6} amplification,⁷ and regeneration⁸ of telecommunication signals to quantum signal processing.⁹ However, there are issues related to this platform that hinder device performance, which are primarily associated with the larger

transmission (both linear and nonlinear) and coupling losses, relative to the fibers. As a result, the on/off parametric gains in the silicon nanophotonic waveguides have been limited to 5.2 dB in the telecom band,⁷ and larger gains (~23 dB) have only been realized by pumping at wavelengths close to the two-photon absorption (TPA) edge ($\lambda \sim 2.2 \mu\text{m}$).¹⁰ Although other semiconductor materials with lower nonlinear losses have been considered for on-chip wavelength conversion or parametric amplification in the telecom band, including hydrogenated amorphous silicon,¹¹ silicon nitride,¹² and III–V materials such as AlGaAs,¹³ there are ongoing challenges to integrating these materials with standard fiber components and pump sources. Alternatively, glassy materials such as chalcogenides¹⁴ and high index doped glass¹⁵ can offer reduced losses, both in terms of transmission and coupling, but they usually require longer device lengths and higher pump powers due to their intrinsic lower refractive indices and nonlinearities.

An emerging platform that combines the benefits of crystalline silicon materials and the fiber geometry is that of the silicon core fibers (SCFs). These SCFs can be produced using standard fiber

drawing tower procedures, allowing for the rapid production of long lengths (hundreds of meters) of material, significantly reducing costs.¹⁶ Moreover, as the SCFs are produced with the core in a polycrystalline form, the fabrication procedures are more flexible than their epitaxially grown waveguide counterparts and, in particular, are well-suited to postprocessing treatments, which can be applied to tailor the core dimensions and material quality.¹⁷ By combining fiber drawing with a subsequent tapering procedure, it has been possible to produce SCFs with submicron cores that have linear losses as low as a few decibels per centimeter, which has allowed for the first demonstration of nonlinear propagation in the crystalline SCF platform in the telecom band.¹⁸ The ability to control the core size through tapering offers two additional benefits. First, it provides a route to engineer the dispersion in the SCFs, which is critical for achieving efficient FWM wavelength conversion. Second, it can be used to tailor the mode properties to improve coupling with conventional fiber components and lasers.¹⁹

In this paper, we make use of a low-loss, dispersion engineered SCF to demonstrate FWM-based parametric amplification with an optical gain as high as 9 dB, using a subpicosecond pump source in the telecom band. The SCF was tapered to have a submicron core diameter (~ 915 nm) over a length of 5 mm, with a zero dispersion wavelength (ZDW) of 1550 nm. Broadband wavelength conversion of more than 260 nm has been demonstrated when pumping the SCF close to the ZDW, just within the normal dispersion regime. Owing to the high coupling efficiency of our tapered design and low propagation losses, a net off-fiber gain of ~ 2 dB is achieved. Furthermore, owing to the larger waveguide dimensions of the SCFs, when compared to the nanophotonic waveguides, no significant saturation of the parametric gain due to nonlinear absorption has been observed up to peak pump powers of ~ 17 W. We anticipate that this SCF platform will be of interest for a range of nonlinear wavelength conversion applications across the telecommunications bands and beyond, particularly where compact, all-fiber integrated devices are desirable.

II. FIBER DESIGN AND EXPERIMENTAL SETUP

Degenerate FWM involves two photons from the pump beam (frequency ω_p) being converted to a signal photon (ω_s) and an idler photon (ω_i) such that $2\omega_p = \omega_s + \omega_i$. The result is optical amplification of the signal and the generation of a frequency converted idler beam. As well as energy conservation, efficient FWM requires minimal phase-mismatch between the pump, signal, and idler waves. For nonlinear processes, the phase-matching condition can be satisfied when

$$\Delta k = 2\gamma P_{\text{pump}} - \Delta k_L = 0, \quad (1)$$

where Δk is the total phase-mismatch, Δk_L is the linear phase-mismatch, and $2\gamma P_{\text{pump}}$ is the nonlinear phase shift, including the effects of self- and cross-phase modulation. In the nonlinear term, P_{pump} is the pump peak power and $\gamma = 2\pi n_2/\lambda_p A_{\text{eff}}$ is the effective nonlinearity parameter, where n_2 is the nonlinear refractive index, λ_p is the pump wavelength, and A_{eff} is the effective mode area. In general, efficient phase-matching occurs close to the ZDW, in which case the linear term can be approximated by²⁰

$$\Delta k_L = -\beta_2 \Delta\omega^2 - \frac{1}{12} \beta_4 \Delta\omega^4, \quad (2)$$

where β_2 is the group velocity dispersion (GVD) term, β_4 is the fourth order dispersion (FOD), and $\Delta\omega$ is the frequency shift between the signal and the pump waves. Depending on the magnitudes and signs of β_2 and β_4 , a variety of phase-matching conditions can be obtained, which result in different conversion bandwidths.²¹ When FOD plays a role, the width of the phase-matching region is obtained from Eq. (2) as²²

$$\Delta\omega = \sqrt{\frac{12|\beta_2|}{|\beta_4|}}, \quad (3)$$

where β_2 and β_4 must be opposite in sign in the normal dispersion regime.

Similar to the nanophotonic silicon waveguides, the GVD of the SCFs can be controlled by reducing the core diameter so that the waveguide dispersion can compensate for the large normal material dispersion. Figure 1 plots the simulated GVD and FOD profiles in the SCFs, with three different core diameters as labeled (see [supplementary material](#), III). The variation in the core size results in a significant shift of the ZDW. For a fixed pump wavelength, which in our case is 1541 nm, the core diameter must be carefully chosen to access the desired dispersion regime and be close to the ZDW. From the dispersion profiles in Fig. 1, we target a SCF with a core diameter of 915 nm, which exhibits a very small positive GVD ($\beta_2 \sim 0.038$ ps² m⁻¹) and a negative FOD ($\beta_4 \sim -0.8 \times 10^{-5}$ ps⁴ m⁻¹) at the pump wavelength. As evident from Eq. (3), this dispersion combination permits broadband phase-matching from the pump with a conversion bandwidth of ~ 380 nm, spanning almost the entire telecom window.^{12,23,24}

The SCFs used in this work were fabricated using the molten core drawing (MCD) method, followed by tapering to reduce the core size, as detailed in Refs. 16, 18, and 25 (see [supplementary material](#), I). Significantly, postprocessing the fibers via tapering is advantageous as it helps improve the material quality of the core,

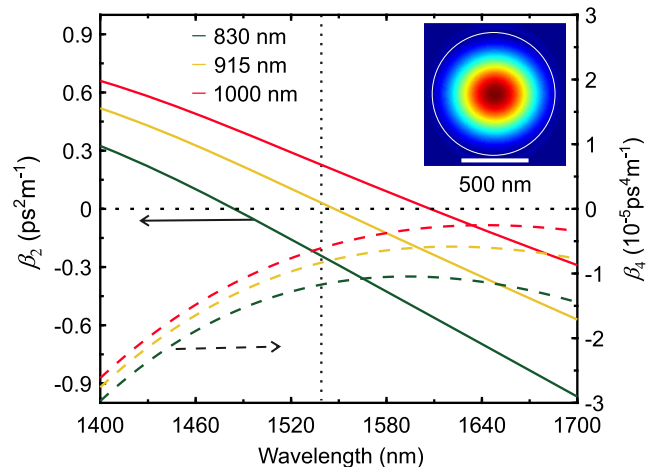


FIG. 1. Calculated GVD and FOD dispersion as a function of wavelength for the SCF with different core diameters shown in the legend. The vertical dash line indicates the pump wavelength. Inset: simulated mode profile of the 915 nm core SCF at the pump wavelength.

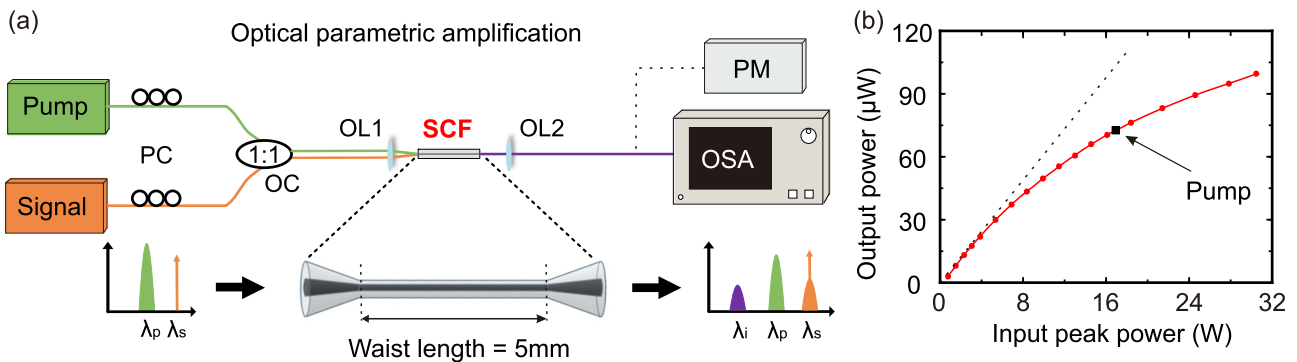


FIG. 2. (a) Schematic of the experimental setup. PC: polarization controller. OC: optical coupler. OL: objective lens. OSA: optical spectrum analyzer. PM: power meter. Inset: symmetric tapered SCF profile. (b) Measured transmission as a function of input peak pump power. The red curve is the simulated transmission including nonlinear loss from TPA. The dashed line (black) indicates the linear insertion loss.

which is polycrystalline in nature, by increasing the grain size.¹⁷ The resulting fiber had input and output core diameters of $4\ \mu\text{m}$, which were tapered down to a waist of $915\ \text{nm}$ over a length of $\sim 5\ \text{mm}$ in the center region, as illustrated in the inset of Fig. 2(a). The total fiber length was $8\ \text{mm}$ including the input and output coupling tapers. The propagation loss of the SCF at the $1541\ \text{nm}$ pump wavelength was estimated to be $\sim 2.8\ \text{dB/cm}$, by subtracting the input $\sim 4\ \text{dB}$ and output $\sim 3\ \text{dB}$ coupling efficiencies from the total $9.2\ \text{dB}$ transmission loss. This propagation loss represents the lowest value reported for a submicron SCF¹⁸ and, indeed, any planar polysilicon waveguide of similar dimensions in the telecom band.²⁶ Moreover, as the crystallinity of the core material has been shown to improve with decreasing diameter,¹⁸ we expect that this loss value represents an upper bound on the loss in the tapered waist, where the nonlinear processing occurs. It is also worth noting that for this SCF design, the light propagating in the fundamental mode is well confined to the core for all diameters, as illustrated in the inset of Fig. 1. Thus, we expect the largest contribution to the losses to be defects and/or impurities in our polysilicon material, as opposed to surface roughness that tends to dominate in planar waveguides,²⁷ and work is ongoing to improve the material quality.

The experimental setup for OPA within our SCF is depicted in Fig. 2(a). The pump source was a mode-locked erbium doped fiber laser emitting pulses centered at $1541\ \text{nm}$ with a $670\ \text{fs}$ full-width at half-maximum (FWHM) duration, corresponding to a $3\ \text{dB}$ spectral bandwidth of $\sim 7\ \text{nm}$ (transform limited), and a repetition rate of $40\ \text{MHz}$. This short pulse pump laser was chosen because the high peak powers are desirable for efficient parametric amplification, while the subpicosecond durations help reduce the number of TPA-induced free carriers that are generated.²⁸ Furthermore, as the free carrier lifetime for submicron silicon waveguides is typically $\sim 1\ \text{ns}$, the modest repetition rate allows the material to recover between pulses, further reducing losses associated with free carrier effects.²⁹ A tunable CW laser was used as the signal beam, with a tuning range covering $1570\text{--}1680\ \text{nm}$. It is worth noting that low power transmission measurements conducted with this source have shown that the linear losses are fairly constant over the entire signal wavelength range, averaging $\sim 3\ \text{dB/cm}$ (see supplementary material, II). Two polarization controllers (PCs) were used

to align the linearly polarized pump and signal beams to optimize the conversion efficiency. The pump and signal were combined by a $3\ \text{dB}$ optical coupler before free space coupling into the SCF. The input coupling was achieved with a microscope objective lens (OL1) with a NA of 0.65 , which was chosen to optimize coupling into the fundamental mode.³⁰ No additional polarizer was needed at the input stage as the cylindrically symmetric SCF is polarization insensitive, which was confirmed by monitoring the output signal power when changing the polarization of the combined input pump and signal beams. The output light was collected by a second microscope objective lens (OL2) with a NA of 0.85 and directed either to a power meter or focused into an optical spectrum analyzer (OSA YOKOGAWA AQ6370D). All the spectra were measured with a $1\ \text{nm}$ resolution bandwidth of the OSA. It is worth noting that, owing to the high nonlinearity and improved coupling efficiency of the tapered SCF platform, we do not require any additional amplification stages for our pump and signal beams, simplifying the setup and helping reduce noise levels.

III. RESULTS

Using the experimental setup, the nonlinear transmission properties of the SCF were first measured at the pump wavelength. Details of the full set of nonlinear parameters for the tapered SCF can be found in supplementary material, III. Figure 2(b) plots the results of the nonlinear absorption measurements, showing the saturation of the output power as a function of coupled input power. In order to minimize the effects of nonlinear absorption and spectral broadening of the pump, a moderate coupled average power of $\sim 0.63\ \text{mW}$ ($\sim 17\ \text{W}$ peak power) was chosen, just below the saturation threshold. As evident from the transmission plot in Fig. 2(b), the total nonlinear loss introduced in the SCF for this pump power was only $\sim 1.5\ \text{dB}$. We attribute the relatively low nonlinear loss measured in our SCF at these coupled power levels to its large mode area, which is more than twice as large as the areas of the nanophotonic waveguides used for FWM in Ref. 7.

Wavelength conversion via OPA was then investigated by simultaneously injecting the pump pulses with low power CW signals ($>1\ \text{mW}$) at different wavelengths. Figure 3(a) shows the optical

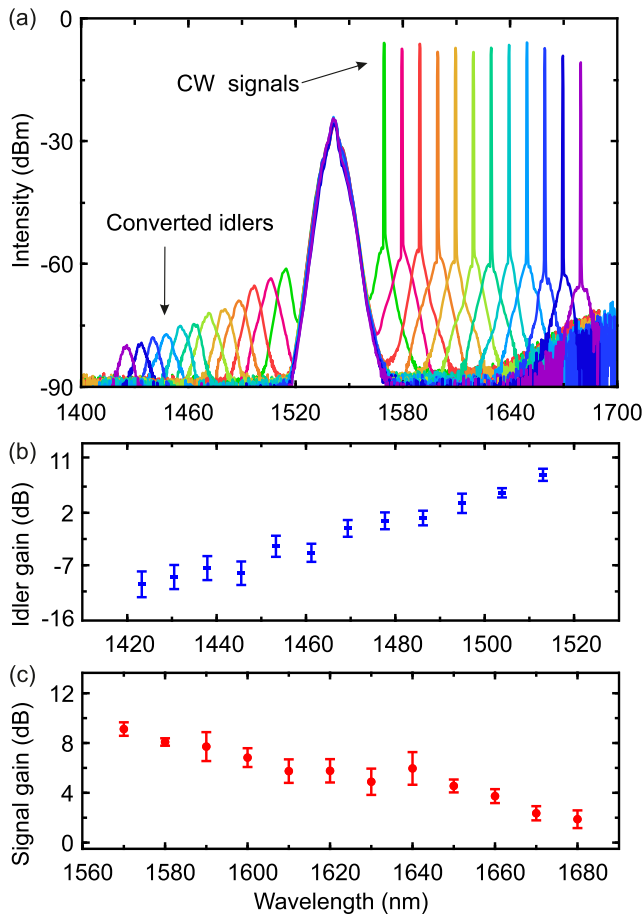


FIG. 3. (a) Transmission spectra taken at the output of the SCF as the signal wavelength is tuned from 1570 to 1680 nm. Idler conversion gain (b) and on/off parametric signal gain (c) as a function of wavelength. The error bars in the parametric gain data are derived from the uncertainty in the total propagation loss and the OSA noise.

spectra generated by the degenerate FWM process, with signal wavelengths from 1570 to 1680 nm overlaid. Owing to the use of a pulsed pump, the amplified signals and generated idlers also occur as a train of short pulses, which is evident from their broad bandwidths. These results clearly show that the signal can be down-converted by ~ 260 nm (32 THz), from 1680 nm to 1420 nm, covering the entire S-, C-, and L- telecom bands. It is important to note that this experimental conversion bandwidth was only limited by the tuning range of our CW source, and it should be possible to extend this over the full ~ 380 nm, as predicted by Eq. (3). Nevertheless, this conversion bandwidth is larger than previous reports of OPA in silicon waveguides using a telecom pulse pump source, thanks to the low GVD, and the bandwidth could be further improved by carefully tailoring the core diameter to reduce the FOD at the pump wavelength.²³

Following the same methods in Refs. 10 and 12, the peak power of the generated idler and signal beams are extracted by converting the time-averaged power measured by the OSA, weighted by the duty cycle factor $F = 1/(40 \text{ MHz} \cdot 670 \text{ fs})$ of our pump laser (see

supplementary material, III). The fiber output coupling efficiency, as calculated for the signal (3 dB) and idler (~ 7.7 dB) wavelengths, is used to obtain the actual converted powers out of the SCF. The on/off parametric signal gain can then be calculated via the ratio $P_{\text{signal,peak}}/P_{\text{signal,out}}$, where $P_{\text{signal,out}}$ is the CW signal power at the output of the SCF with the pump off. The on/off parametric idler conversion gain is calculated via the ratio $P_{\text{idler,peak}}/P_{\text{signal,out}}$. The extracted values of the parametric signal gain and idler conversion gain are plotted in Figs. 3(b) and 3(c), respectively. The experimental data reveal that a large maximum on/off signal gain of ~ 9 dB is achieved at a wavelength of 1570 nm, with a corresponding idler conversion gain of ~ 8.5 dB. Such a large on/off parametric signal gain in our tapered SCF is sufficient to overcome the moderate fiber insertion losses (7 dB), demonstrating a 2 dB net off-waveguide gain. The maximum signal gain obtained in our 8 mm long SCF exhibits more than a 3 dB improvement over the current highest record in a 17 mm nanophotonic silicon waveguide in the telecom band, which was obtained with a picosecond pulsed pump.⁷ We attribute this increased gain to the lower overall losses in our system, which is due in part to the larger core size of the fiber and also the reduced free carrier absorption associated with our shorter pump pulses (see supplementary material, III). For both the signal and idler beams, the gains decrease as the signal wavelength moves away from the pump, which follows the theoretical predictions for waveguides pumped in the normal dispersion region.^{20,31} Although the maximum measured idler conversion gain is also higher than previous reports, it is slightly lower than the signal gain, which we attribute to the larger linear losses at the shorter wavelengths for polysilicon fibers.³²

Additional experiments were carried out to investigate the gain dynamics with the signal wavelength set at $\lambda = 1590$ nm so that both the signal and idler beams were far away from the pump bandwidth. In the regime of negligible nonlinear losses, the parametric gain should remain constant when the signal power is varied. This can be seen from the linearly increasing trend of the idler and signal output powers as the coupled signal power is raised from -3 to 1.3 dBm, as shown by the black lines in Figs. 4(a) and 4(b), respectively. The slope efficiency, plotted as the red curves in Figs. 4(a) and 4(b), represent the idler and signal gains as a function of power, which yield values of ~ 4.8 dB and ~ 6.5 dB, with a fluctuation of less than 1 dB. These measurements reveal that there is no significant gain saturation in our SCF for peak pump powers up to ~ 17 W, which are easily attainable using conventional cost-effective fiber lasers, and the powers could be reduced further by increasing the SCF length.

As a final comment, in order to understand the relationship between the on/off parametric signal gain and the dispersion properties of our SCF, the measured gain is replotted as a function of signal wavelength in Fig. 4(c) (red squares). This gain distribution can be compared with the theoretical predictions for the signal gain as¹

$$G_{\text{signal}} = \frac{P_{\text{signal, out}}}{P_{\text{signal, in}}} = 1 + \left[\frac{\gamma P_{\text{pump}}}{g} \sinh(gL_{\text{eff}}) \right]^2, \quad (4)$$

where L_{eff} is the effective fiber length, taking into account the linear propagation loss, and the parametric gain coefficient g is given by $g = \sqrt{\gamma P_{\text{pump}} \Delta k_L - (\Delta k_L/2)^2}$.

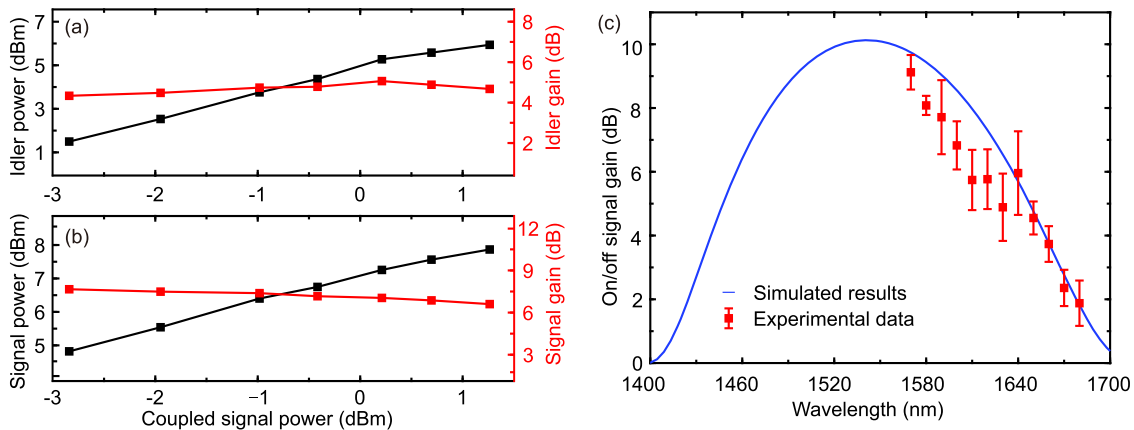


FIG. 4. (a) Measured amplified idler power (black) and conversion gain (red) as a function of signal power (1590 nm) at the SCF output. (b) Measured signal power (black) and gain (red) as a function of signal power (1590 nm) at the SCF output. (c) Calculated (blue solid line) and measured (red squares) on/off signal gain as a function of signal wavelength, using a pump with ~ 17 W peak power centered at 1541 nm.

The signal gain was calculated by substituting the values $\gamma = 40.77 \text{ W}^{-1} \text{ m}^{-1}$, $P_{\text{pump}} = 17 \text{ W}$, and $L_{\text{eff}} = 4.4 \text{ mm}$, and the dispersion parameters (β_2 and β_4) into Eq. (4). However, instead of fixing the values of β_2 and β_4 to those obtained from Fig. 1, here we leave them as free parameters to achieve the best fit to the experimental data. The blue curve plotted in Fig. 4(c) was obtained with the values $\beta_2 \sim 0.042 \text{ ps}^2 \text{ m}^{-1}$ and $\beta_4 \sim -0.3 \times 10^{-5} \text{ ps}^4 \text{ m}^{-1}$, corresponding to a coefficient of determination $R^2 \sim 0.8$,³³ which agree well with the calculated dispersion parameters, assuming the target core diameter of 915 nm. We attribute the discrepancy between the fitted curve and the measured gain at the wavelengths close to the central frequency of the pump to difficulties in calculating the peak signal power when the signal and pump bandwidths overlap, resulting in an underestimation of the gain in this region. Nevertheless, such close agreement is quite remarkable when we consider how sensitive these values are to the precise core size in such a high-index contrast waveguide and that we are approximating the dispersion of our polysilicon core material with that of single crystal silicon. Thus, these results are further evidence of the high quality of the SCF core materials and our ability to precisely control the dimensions of the tapered profiles.

IV. CONCLUSION

In this work, we report optical parametric amplification in the telecom band using a low-loss SCF that has been tapered down to have a submicron core diameter. Owing to the high coupling efficiency and negligible nonlinear absorption in the SCF, a signal gain as high as 9 dB was achieved with a moderate pump peak power of 17 W. To the best of our knowledge, this is the highest parametric gain reported in a crystalline silicon waveguide using subpicosecond pump pulses at a telecommunications wavelength, resulting in the first demonstration of net off-waveguide gain in this regime. The experimentally measured conversion bandwidth of $\sim 260 \text{ nm}$ covers the entire S-, C-, and L- telecom bands, and this could be extended further with careful design of our tapered structure. We expect that continued efforts to reduce the transmission losses and exploit the low-loss splicing methods of the SCFs with conventional silica fibers

will significantly improve the practicality of this platform, opening a route for the development of compact and efficient all-fiber nonlinear signal processing systems.

SUPPLEMENTARY MATERIAL

See [supplementary material](#) for the fabrication and postprocessing of SCFs, transmission characterizations, simulation parameters, and parametric gain analysis.

ACKNOWLEDGMENTS

This publication was supported by the following research funds: the Engineering and Physical Sciences Research Council (EPSRC) (Grant No. EP/P000940/1); the National Natural Science Foundation of China (NSFC) (Grant No. 61705072); the Norwegian Research Council (Grant No. 262232); and the J. E. Sirrine Foundation. The data for this work are accessible through the University of Southampton Institutional Research Repository (<https://doi.org/10.5258/SOTON/D1014>).

REFERENCES

- J. Hansryd, P. A. Andrekson, M. Westlund, and P. Hedekvist, "Fiber-based optical parametric amplifiers and their applications," *IEEE J. Sel. Top. Quantum Electron.* **8**, 506–520 (2002).
- M. Onishi, T. Okuno, T. Kashiwada, S. Ishikawa, N. Akasaka, and M. Nishimura, "Highly nonlinear dispersion-shifted fibers and their application to broadband wavelength converter," *Opt. Fiber Technol.* **4**, 204–214 (1998).
- J. Leuthold, C. Koos, and W. Freude, "Nonlinear silicon photonics," *Nat. Photonics* **4**, 535–544 (2010).
- R. L. Espinola, J. I. Dadap, R. M. Osgood, S. J. McNab, and Y. A. Vlasov, "C-band wavelength conversion in silicon photonic wire waveguides," *Opt. Express* **13**, 4341–4349 (2005).
- H. Fukuda, K. Yamada, T. Shoji, M. Takahashi, T. Tsuchizawa, T. Watanabe, J. Takahashi, and S. Itabashi, "Four-wave mixing in silicon wire waveguides," *Opt. Express* **13**, 4629–4637 (2005).

- ⁶H. Rong, Y. Kuo, A. Liu, M. Paniccia, and O. Cohen, "High efficiency wavelength conversion of 10Gb/s data in silicon waveguides," *Opt. Express* **14**, 1182–1188 (2006).
- ⁷M. A. Foster, A. C. Turner, J. E. Sharping, B. S. Schmidt, M. Lipson, and A. L. Gaeta, "Broad-band optical parametric gain on a silicon photonic chip," *Nature* **441**, 960–963 (2006).
- ⁸R. Salem, M. A. Foster, A. C. Turner, D. F. Geraghty, M. Lipson, and A. L. Gaeta, "Signal regeneration using low-power four-wave mixing on silicon chip," *Nat. Photonics* **2**, 35–38 (2008).
- ⁹K. Harada, H. Takesue, H. Fukuda, T. Tsuchizawa, T. Watanabe, K. Yamada, Y. Tokura, and S. Itabashi, "Frequency and polarization characteristics of correlated photon-pair generation using a silicon wire waveguide," *IEEE J. Sel. Top. Quantum Electron.* **16**, 325–331 (2010).
- ¹⁰X. Liu, R. M. Osgood, Jr., Y. A. Vlasov, and W. M. J. Green, "Mid-infrared optical parametric amplifier using silicon nanophotonic waveguides," *Nat. Photonics* **4**, 557–560 (2010).
- ¹¹B. Kuyken, S. Clemen, S. K. Selvaraja, W. Bogaerts, D. V. Thourhout, P. Emplit, S. Massar, G. Roelkens, and R. Baets, "On-chip parametric amplification with 26.5 dB gain at telecommunication wavelengths using CMOS-compatible hydrogenated amorphous silicon waveguides," *Opt. Lett.* **36**, 552–554 (2011).
- ¹²K. J. A. Ooi, D. K. T. Ng, T. Wang, A. K. L. Chee, S. K. Ng, Q. Wang, L. K. Ang, A. M. Agarwal, L. C. Kimerling, and D. T. H. Tan, "Pushing the limits of CMOS optical parametric amplifiers with USRN: Si₃N₄ above the two-photon absorption edge," *Nat. Commun.* **8**, 13878 (2017).
- ¹³M. Pu, H. Hu, L. Ottaviano, E. Semenova, D. Vukovic, L. K. Oxenlowe, and K. Yvind, "Ultra-efficient and broadband nonlinear AlGaAs-on-Insulator chip for low-power optical signal processing," *Laser Photonics Rev.* **12**, 1800111 (2018).
- ¹⁴B. J. Eggleton, B. Luther-Davies, and K. Richardson, "Chalcogenide photonics," *Nat. Photonics* **5**, 141–148 (2010).
- ¹⁵F. Da Ros, E. P. da Silva, D. Zibar, S. T. Chu, B. E. Little, R. Morandotti, M. Galili, D. J. Moss, and L. K. Oxenlowe, "Wavelength conversion of QAM signals in a low loss CMOS compatible spiral waveguide," *APL Photonics* **2**, 046105 (2017).
- ¹⁶J. Ballato, T. Hawkins, P. Foy, R. Stolen, B. Kokuoz, M. Ellison, C. McMillen, J. Reppert, A. M. Rao, M. Daw, S. Sharma, R. Shori, O. Stafsudd, R. R. Rice, and D. R. Powers, "Silicon optical fiber," *Opt. Express* **16**, 18675–18683 (2008).
- ¹⁷Y. Franz, A. F. J. Runge, H. Ren, N. Healy, K. Ignatyev, M. Jones, T. Hawkins, J. Ballato, U. J. Gibson, and A. C. Peacock, "Material properties of tapered crystalline silicon core fibers," *Opt. Mater. Express* **7**, 2055–2061 (2017).
- ¹⁸F. H. Suhailin, L. Shen, N. Healy, L. Xiao, M. Jones, T. Hawkins, J. Ballato, U. J. Gibson, and A. C. Peacock, "Tapered polysilicon core fibers for nonlinear photonics," *Opt. Lett.* **41**, 1360–1363 (2016).
- ¹⁹H. Ren, O. Aktas, Y. Franz, A. F. J. Runge, T. Hawkins, J. Ballato, U. J. Gibson, and A. C. Peacock, "Tapered silicon core fibers with nano-spikes for optical coupling via spliced silica fibers," *Opt. Express* **25**, 24157–24163 (2017).
- ²⁰R. J. Kruhlak, G. K. Wong, J. S. Chen, S. G. Murdoch, R. Leonhardt, J. D. Harvey, N. Y. Joly, and J. C. Knight, "Polarization modulation instability in photonic crystal fibers," *Opt. Lett.* **31**, 1379–1381 (2006).
- ²¹X. Liu, B. Kuyken, G. Roelkens, R. Baets, R. M. Osgood, Jr., and W. M. J. Green, "Bridging the mid-infrared-to-telecom gap with silicon nanophotonic spectral translation," *Nat. Photonics* **6**, 667–671 (2012).
- ²²M. A. Foster, A. C. Turner, R. Salem, M. Lipson, and A. L. Gaeta, "Broad-band continuous-wave parametric wavelength conversion in silicon nanowaveguides," *Opt. Express* **15**, 12949–12958 (2007).
- ²³A. C. Turner-Foster, M. A. Foster, R. Salem, A. L. Gaeta, and M. Lipson, "Frequency conversion over two-thirds of an octave in silicon nanowaveguides," *Opt. Express* **18**, 1904–1908 (2010).
- ²⁴B. Kuyken, P. Verheyen, P. Tannouri, X. Liu, J. V. Campenhout, R. Baets, W. M. J. Green, and G. Roelkens, "Generation of 3.6 μm radiation and telecom-band amplification by four-wave mixing in a silicon waveguide with normal group velocity dispersion," *Opt. Lett.* **39**, 1349–1352 (2014).
- ²⁵E. F. Nordstrand, A. N. Dibbs, A. J. Eraker, and U. J. Gibson, "Alkaline oxide interface modifiers for silicon fiber production," *Opt. Mater. Express* **3**, 651–657 (2013).
- ²⁶D. Kwong, J. Covey, A. Hosseini, Y. Zhang, X. Xu, and R. T. Chen, "Ultralow-loss polycrystalline silicon waveguides and high uniformity $1 \times 12\text{MMI}$ fanout for 3D photonic integration," *Opt. Express* **20**, 21722–21728 (2012).
- ²⁷K. P. Yap, A. Delage, J. Lapointe, B. Lamontagne, J. H. Schmid, P. Waldron, B. A. Syrett, and S. Janz, "Correlation of scattering loss, sidewall roughness and waveguide width in silicon-on-insulator (SOI) ridge waveguides," *J. Light. Technol.* **27**, 3999–4008 (2009).
- ²⁸X. Sang and O. Boyraz, "Gain and noise characteristics of high-bit-rate silicon parametric amplifiers," *Opt. Express* **16**, 13122–13132 (2008).
- ²⁹I. Aldaya, A. Gil-Molina, J. L. Pita, L. H. Gabrielli, H. L. Fragnito, and P. Dainese, "Nonlinear carrier dynamics in silicon nano-waveguides," *Optica* **4**, 1219–1227 (2017).
- ³⁰A. C. Peacock, P. Mehta, P. Horak, and N. Healy, "Nonlinear pulse dynamics in multimode silicon core optical fibers," *Opt. Lett.* **37**, 3351–3353 (2012).
- ³¹Q. Lin, J. Zhang, P. M. Fauchet, and G. P. Agrawal, "Ultrabroadband parametric generation and wavelength conversion in silicon waveguides," *Opt. Express* **14**, 4786–4799 (2006).
- ³²S. Chaudhuri, J. R. Sparks, X. Ji, M. Krishnamurthi, L. Shen, N. Healy, A. C. Peacock, V. Gopalan, and J. V. Badding, "Crystalline silicon optical fibers with low optical loss," *ACS Photonics* **3**, 378–384 (2016).
- ³³S. M. Ross, *Introductory Statistics*, 3rd ed. (Academic Press, 2010).